AIP | Applied Physics Letters

Micromachined piezoelectric ultrasonic transducer with ultra-wide frequency bandwidth

Tao Wang, Takeshi Kobayashi, and Chengkuo Lee

Citation: Applied Physics Letters **106**, 013501 (2015); doi: 10.1063/1.4905441
View online: http://dx.doi.org/10.1063/1.4905441
View Table of Contents: http://scitation.aip.org/content/aip/journal/apl/106/1?ver=pdfcov
Published by the AIP Publishing

Micromachined piezoelectric ultrasonic transducer with ultra-wide frequency bandwidth

Tao Wang,[1] Takeshi Kobayashi,[2] and Chengkuo Lee[1,a)]
[1]*Department of Electrical and Computer Engineering, National University of Singapore, 4 Engineering Drive 3, Singapore 11757*
[2]*National Institute of Advanced Industrial Science and Technology (AIST), 1-2-1 Namiki, Tsukuba, Ibaraki 305-8564, Japan*

(Received 25 September 2014; accepted 20 December 2014; published online 5 January 2015)

An ultrasonic transducer with a wide frequency bandwidth is always preferred for diagnostic ultrasound imaging, because a wide frequency bandwidth can reduce the duration of an ultrasonic pulse and enhance the axial imaging resolution. However, the frequency bandwidth of both conventional ultrasonic transducer and normal piezoelectric micromachined ultrasonic transducer (pMUT) is quite limited. To overcome this limitation, the mode-merging pMUT is presented in this letter. By using the rectangular membrane with large length/width aspect ratio, several resonant modes are excited within a narrow frequency range. When this pMUT works in a largely damped medium, excited modes are merged together and result in an ultra-wide bandwidth. A −6 dB bandwidth of 95% is measured in water for the proposed pMUT without matching layer, which is much broader than that of conventional pMUTs. Benefited from such ultra-wide frequency bandwidth, the pulse duration of 1 μs is achieved at a central frequency of 1.24 MHz. If this ultra-wide bandwidth pMUT is utilized to replace the conventional transducer for diagnostic ultrasound imaging, the axial resolution can be significantly enhanced without compromising imaging depth. © *2015 AIP Publishing LLC*. [http://dx.doi.org/10.1063/1.4905441]

Ultrasound based diagnostic imaging is widely used for visualizing internal body structures. It is efficient, low-cost, and real-time, and does not have any harmful ionizing radiation. For diagnostic imaging, the axial imaging resolution equals to half of spatial ultrasonic pulse length, and shorter pulse length results in better resolution.[1] The ultrasonic pulses are transmitted and received by an ultrasonic transducer. Shorter pulse length can be achieved by increasing the operating frequency. However, higher frequency leads to higher attenuation and the detecting range becomes very small. To ensure a reasonable detecting range, the highest frequency is usually below 10 MHz.[2] Another way to achieve shorter pulse length is to increase the frequency bandwidth of ultrasonic transducer. When an ultrasonic transducer is excited by a short electric pulse, it rings at the resonant frequency for a few oscillations. Therefore, the generated acoustic pulse cannot be ideally shortened. If Fourier Transform is applied to the pulse, a dispersion of frequency can be observed. The pulse actually contains a series of frequencies, and the frequencies spread more for shorter pulse. Since the pulse length is inversely proportional to the frequency bandwidth,[3] an ultrasonic transducer with wide frequency bandwidth can generate very short pulses, which means the resolution can be further enhanced. On the other hand, image resolution can be maintained if frequency is moderately decreased to increase the detecting range. Furthermore, if the frequency bandwidth is wide enough, advanced harmonic sensing technology can be realized by a single device. It will significantly enhance the imaging contrast.[2] Therefore, ultrasonic transducer with large frequency bandwidth is always preferred.

Ultrasonic transducers made of bulk piezoelectric ceramics have been dominant approaches for decades, but its limited bandwidth can hardly meet the requirement. The limited bandwidth is mainly due to the large acoustic impedance mismatch between the transducer and soft tissue of human body. By using microelectromechanical system (MEMS) technology, the micromachined ultrasonic transducer (MUT) is a promising solution, which aims to overcome the shortcomings of ultrasonic transducers based on bulk piezoelectric ceramics. The flexural mode operation of MUT significantly reduces its mechanical impedance, minimizing the acoustic impedance mismatch between the transducer and working medium. This concept has been realized using capacitive sensing and actuating mechanism, known as capacitive MUT (cMUT). A remarkably wide frequency bandwidth of over 100% has been achieved without any matching layer.[4] However, the operating voltage of cMUT is extremely high, e.g., over 100 V. Such high voltage creates safety concerns and limits possible applications of cMUT. As an alternative, piezoelectric MUT (pMUT) is driven using piezoelectric effect, which enables pMUTs operate at a much lower voltage in comparison to cMUTs. Similar to cMUTs, pMUTs work in the flexural plate mode, therefore the acoustic impedance of pMUTs is expected to be lowered as well.[5] Unfortunately, performances of the reported pMUTs are much poorer than expectation, especially for the bandwidth. Despite of analytical modeling with a possible bandwidth of over 100% for pMUT,[6] experimental results show that the bandwidth of pMUT is much smaller than this ideal value and even worse than conventional bulk

a)Author to whom correspondence should be addressed. Electonic address: elelc@nus.edu.sg

piezoelectric ceramic based ultrasonic transducer.[7,8] Such deviation is mainly attributed to the residual stress after high temperature processing. Although Muralt *et al*. implements a pMUT with flat membrane by stresses compensation, the bandwidth is severely limited. As the conclusion given by the authors, pMUT should not be used for applications requiring wide bandwidth.[9]

To overcome the bandwidth limitation of pMUT, Hajati *et al*. develop a pMUT array with elements of different sizes and distinct resonant peak.[10] When these elements work together in water, all the peaks are merged and form a wide bandwidth. Although the bandwidth issue is addressed, the broadband effect is achieved by leveraging the whole array. Wide bandwidth of an individual pixel is still not available, and ultrasonic image cannot be obtained without mechanically scanning. In this letter, we propose a mode-merging pMUT device. This pMUT contains a rectangular plate with a large aspect ratio, of which the first a few resonant frequencies are close to each other. When the pMUT operates in largely damped medium like water or soft tissue, the resonant peaks of different modes are merged together, forming a much wider bandwidth. A −6 dB bandwidth of over 94% is achieved by a single pMUT in water without matching layer. The associate pulse duration is only 1 μs at central frequency of 1.24 MHz, which is considerably shorter than previously reported pMUTs.

Figure 1(a) shows the schematic illustration of the mode-merging pMUT containing a released rectangular plate. Choi *et al*. developed 1-D and 2-D analytical models to describe the behavior of pMUT with rectangular plate, but such models only consider the fundamental mode.[11,12] Since the proposed pMUT employs several resonant modes merged together, such analytical models may not be suitable. To calculate its modal frequencies, the pMUT is modeled as a rectangular membrane (dimensions: L_x and L_y) with fully clamped boundaries. Such membrane is assumed to be composed by uniform material for simplification. The modal frequencies of the membrane are given by[13]

$$f_{m,n} = \frac{1}{2} \times \sqrt{\frac{T}{\sigma}} \times \sqrt{\frac{m^2}{{L_x}^2} + \frac{n^2}{{L_y}^2}} \quad m, n = 1, 2, 3, \ldots, \tag{1}$$

where T is the surface tension, and σ is the area density.

Considering k as the length/width aspect ratio ($k = L_x/L_y$ and $L_y = L$), Eq. (1) then can be rewritten as

$$f_{m,n} = \frac{1}{2L} \times \sqrt{\frac{T}{\sigma}} \times \sqrt{\left(\frac{m^2}{k^2} + n^2\right)} \quad m, n = 1, 2, 3, \ldots. \tag{2}$$

The fundamental frequency f_0 ($m = 1$, $n = 1$) thus is

$$f_0 = \frac{1}{2L} \times \sqrt{\frac{T}{\sigma}} \times \sqrt{\left(\frac{1}{k^2} + 1\right)} \tag{3}$$

and the modal frequencies become

$$f_{m,n} = f_0 \times \sqrt{\left(\frac{m^2 + k^2 n^2}{k^2 + 1}\right)} \quad m, n = 1, 2, 3, \ldots. \tag{4}$$

If we consider the frequency of *a-th* vibration mode equals to $f_{1,2}$, then frequencies of first $a - 1$ modes are

$$f_{m,1} = f_0 \times \sqrt{\left(\frac{m^2 + k^2}{k^2 + 1}\right)} \quad m < a. \tag{5}$$

The relation between a and k is shown in Figure 1(b). Once the aspect ratio k is greater than 3, which is usually true for a

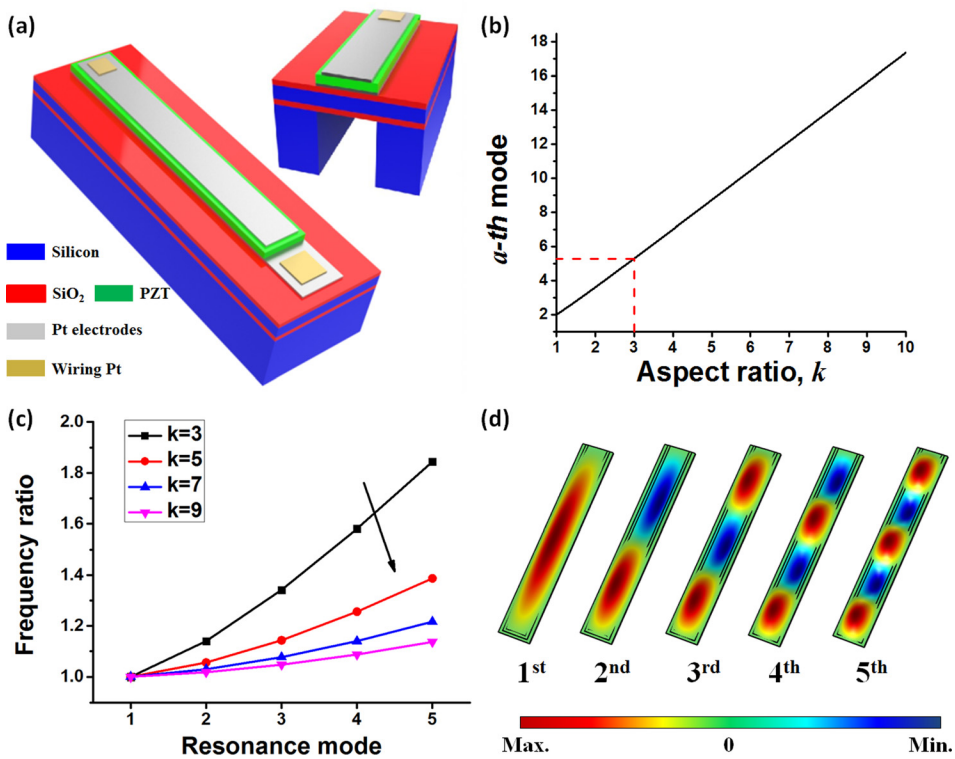

FIG. 1. (a) The schematic drawing of proposed pMUT; (b) relation between a and length/width aspect ratio k; (c) derived modal frequency ratios with varying k and; and (d) the associated mode shapes.

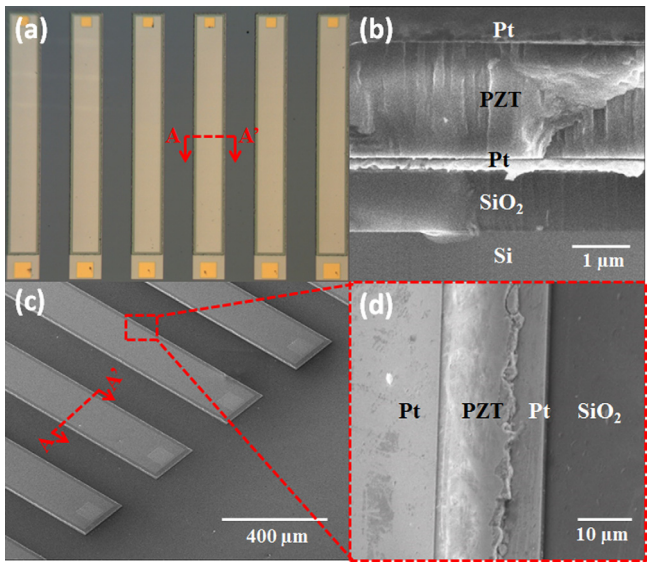

FIG. 2. (a) OM image of fabricated pMUT; SEM image of (b) cross-sectional view of released multi-layer membrane; (c) pMUT array and; and (d) edge of pMUT element.

rectangular membrane, Eq. (5) is valid for the first 5 modes. Hence, the 1st to 5th modes are investigated in this work. Figure 1(c) shows the modal frequency ratios with varying k, and the associated mode shapes are shown in Figure 2(d). The frequency increasing speed is found to be dependent on the parameter k. With higher k, the increasing speed becomes slower, i.e., higher mode frequencies are closer to fundamental frequency. The number of modes which fall into a certain frequency range is controlled by parameter k. Therefore, the length/width aspect ratio k is the key design parameter for the mode-merging pMUT.

The proposed pMUT contains a $1550\,\mu m \times 250\,\mu m$ membrane, with a large length/width aspect ratio k of 6.2. Such high k ensures that the frequency ratios of first 5 modes are less than 1.3. The microfabrication process starts with a multilayer deposition on a silicon-on-insulator (SOI) wafer with 10 μm device layer, 1 μm buried oxide layer (BOX), and 400 μm Si handle layer. A 1 μm oxide layer is initially sputtered on the Si device layer for insulation. Then, the Pt (200 nm)/Ti (10 nm) thin films are deposited by DC magnetron sputtering as the bottom electrode. A layer of 2 μm piezoelectric PZT film is formed using sol-gel process.[14–16] The deposited film is then pyrolyzed and crystallized by rapid thermal annealing. After that Pt (200 nm)/Ti (10 nm) thin films are sputtered again to form the top electrode. The top and bottom platinum electrodes are patterned by Ar ions, while the PZT film is wet-etched using a mixture of HF, HNO_3, and HCl. The Si substrate is finally etched by deep reactive-ion etching (DRIE) down to the BOX layer to release the membrane structure. The optical microscopy (OM) and secondary electron microscopy (SEM) images of the fabricated pMUT are shown in Figure 2. Because of the wet etching process, the edges of PZT thin film are not smooth, illustrated in Figure 2(d).

A 3-D finite elements piezoelectric device model (FEM) is created using COMSOL multi-physics software to study the behavior of this multilayer membrane. The frequency response of displacement amplitude under electrical excitation (1 V_{pp}) is shown in Figure 3(a). As is aforementioned, the low-frequency ultrasound suffers lower attenuation and enables a larger imaging depth. Therefore, the proposed pMUT has a relatively low fundamental frequency (~1.12 MHz). It is worth noting that the even modes are missing in the response spectrum. For an example of 2nd mode, the membrane can be divided into two regions. These two regions are symmetrical with opposite motions. However, the mechanical force from converse piezoelectric effect is unidirectional. The unidirectional force can hardly be coupled to such opposite motion and excite the 2nd mode. Other even modes are also missing for the same reason; hence, only odd modes are electrically excited. Figure 3(b) shows the mode shape at each peak in response spectrum. Totally, three modes are excited within a very narrow frequency range (~0.3 MHz), which is coherent with the

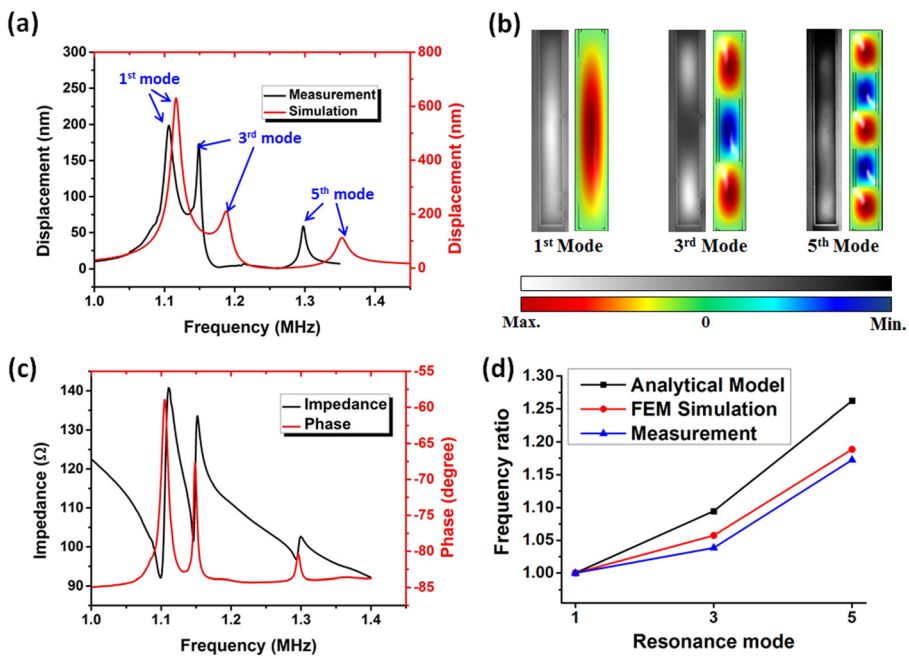

FIG. 3. (a) Measured and simulated frequency response under 1 V_{pp} electrical excitation; (b) the mode shape for each resonant peak. Left ones are measured and right ones are obtained by simulation; (c) impedance measurement results; and (d) comparison of analytical model, FEM simulation and measurement results. (Multimedia view) [URL: http://dx.doi.org/10.1063/1.4905441.1] [URL: http://dx.doi.org/10.1063/1.4905441.2] [URL: http://dx.doi.org/10.1063/1.4905441.3]

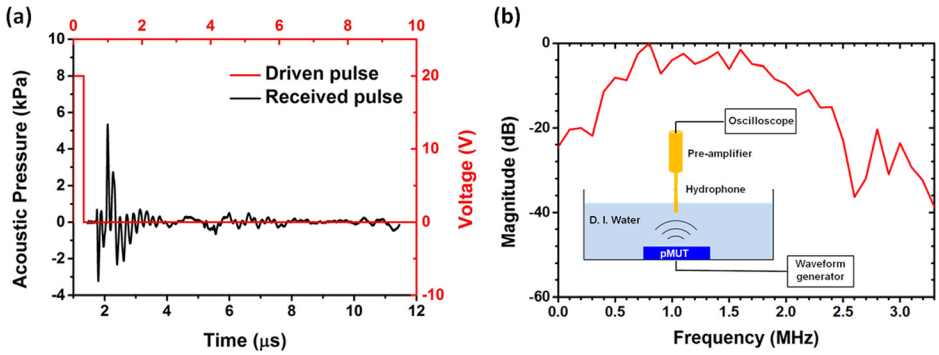

FIG. 4. (a) Underwater performance testing results using hydrophone and (b) the corresponding FFT spectrum. The testing set-up is shown in the inset.

analytical model. The 1st mode and 3rd mode have already merged without considering damping effects from environment. When this pMUT works in largely damped medium, all the three resonance modes, or even more modes, will be merged together, and hence, the frequency bandwidth is significantly broadened.

The fabricated pMUT is first characterized using DHM-R2100 holographic MEMS analyzer by Lyncée Tec Ltd. The device under test (DUT) is electrically excited by the stroboscopic module with 1 V_{pp}. Dynamic 3-D vibrations of DUT are captured and recorded for analysis. Measured frequency response and mode shapes at resonant peaks are shown in Figures 3(a) and 3(b), respectively. Similar to the simulation results, totally three modes are excited within a narrow frequency range of 0.3 MHz with 1st mode and 3rd mode overlapped. It is clearly shown that excited modes are all odd modes, which are consistent with the simulation results and above discussion. Compared with simulation results, the measured frequencies are slightly lower. This may be due to the non-perfect DRIE process during micro-fabrication. Since the side walls cannot be perfectly vertical to the back surface of membrane after DRIE process, therefore, a larger released membrane results in lower frequencies. Another deviation is that measured displacement amplitude of the 1st mode is much smaller than that in simulation. Because the device is characterized in air, the 1st mode may suffer severe air damping. From the measured response spectrum, peak of the 1st mode is observed to be broadened, implying its energy dissipation due to air damping is higher than the 3rd mode. Hence, the displacement amplitude of the 1st mode drops to almost the same as the 3rd mode. The impedance characterization is performed as well using Agilent 4294 A precision impedance analyzer as shown in Figure 3(c). The electromechanical coupling coefficient k_{eff}^2 can be derived by resonant frequency f_r and anti-resonant frequency f_a through following relation:[17]

$$k_{eff}^2 = \frac{f_a^2 - f_r^2}{f_r^2}. \quad (6)$$

Calculated electromechanical coupling coefficients for the 1st, 3rd, and 5th modes are 1.97%, 1.04%, and 0.99%, respectively.

Comparison of analytical model, FEM simulation and measurement are illustrated in Figure 3(d). In general, both the analytical and FEM match the measured data well. Although the analytical model is simplified based on the assumption of a uniformly single layer membrane, the predicted frequencies are slightly higher and the errors are still within acceptable range (5.4% for the 3rd mode and 7.6% for the 5th mode). The analytical model thus provides a quick way to determine the length/width aspect ratio k for design of mode-merging pMUT. For the sophisticated FEM simulation, the results are very close to the experimental data, better than the analytical model. The slight deviation is probably due to some non-ideal factors, as it is discussed above.

To characterize the underwater performance of the fabricated pMUT, a 1.0 mm needle hydrophone along with 8 dB pre-amplifier by Precision Acoustics Ltd. is used to detect the transmitted acoustic pulse at a distance of 3 mm as shown in inset of Figure 4(b). The pMUT is driven by a 20 V electrical pulse signal using an Agilent 33510B waveform generator. Duration of this pulse signal is 300 ns. Driven pulse and received pulse are shown in Figure 4(a), while the corresponding Fast Fourier Transform (FFT) spectrum is shown in Figure 4(b). The −6 dB frequency bandwidth is measured as 95% with central frequency of 1.24 MHz, which is significantly higher than reported data of 10%,[8] 43%,[18] and 57%.[7] Benefited from such ultra-wide frequency bandwidth, the mode-merging pMUT is able to generate very short ultrasonic pulse (1 μs) at relatively low frequency. The pMUT with similar pulse duration (~0.7 μs) operates at much higher frequency of 7.1 MHz.[7] For the pMUT with similar operating frequency (~1.8MHz), its pulse duration is as long as 3 μs.[8] Therefore, the ultra-wide frequency bandwidth pMUT is superior to normal pMUTs.

In this letter, a mode-merging pMUT is designed, fabricated and characterized. Totally, three modes are excited within a narrow frequency range of 0.3 MHz. When this pMUT is working in a highly damped medium, excited modes are merged together and form an ultra-wide frequency bandwidth. The −6 dB bandwidth in water is measured as 95%, which is significantly higher than previously reported pMUTs. Benefited from such ultra-wide frequency bandwidth, 1 μs ultrasonic pulse is achieved at central frequency of 1.24 MHz. Diagnostic imaging with better axial resolution and larger imaging depth may be realized with this ultra-wide frequency bandwidth pMUT.

This work was supported by the Agency for Science, Technology and Research (A*STAR) under Science and Engineering Research Council (SERC) Grant No. 1220103064.

[1]N. M. Tole and H. Ostensen, *Basic Physics of Ultrasonographic Imaging* (World Health Organization, 2005).
[2]P. R. Hoskins, K. Martin, and A. Thrush, *Diagnostic Ultrasound: Physics and Equipment* (Cambridge University Press, 2010).
[3]B. Angelsen, *Ultrasound Imaging: Waves, Signals, and Signal Processing* (Emantec, 2000).
[4]B. T. Khuri-Yakub and Ö. Oralkan, J. Micromech. Microeng. **21**(5), 054004 (2011).
[5]B. Chen, F. Chu, X. Liu, Y. Li, J. Rong, and H. Jiang, Appl. Phys. Lett. **103**(3), 031118 (2013).
[6]F. Akasheh, T. Myers, J. D. Fraser, S. Bose, and A. Bandyopadhyay, Sens. Actuators, A **111**(2), 275 (2004).
[7]D. E. Dausch, J. B. Castellucci, D. R. Chou, and O. T. von Ramm, IEEE Trans. Ultrason. Ferroelectr. Freq. Control **55**(11), 2484 (2008).
[8]G. Percin and B. T. Khuri-Yakub, IEEE Trans. Ultrason. Ferroelectr. Freq. Control **49**(5), 585 (2002).
[9]P. Muralt, N. Ledermann, J. Paborowski, A. Barzegar, S. Gentil, B. Belgacem, S. Petitgrand, A. Bosseboeuf, and N. Setter, IEEE Trans. Ultrason. Ferroelectr. Freq. Control **52**(12), 2276 (2005).
[10]A. Hajati, D. Latev, D. Gardner, A. Hajati, D. Imai, M. Torrey, and M. Schoeppler, Appl. Phys. Lett. **101**(25), 253101 (2012).
[11]H. S. Choi, J. L. Ding, A. Bandyopadhyay, M. J. Anderson, and S. Bose, J. Micromech. Microeng. **18**(2), 025037 (2008).
[12]H. S. Choi, M. J. Anderson, J. L. Ding, and A. Bandyopadhyay, J. Micromech. Microeng. **20**(1), 015013 (2010).
[13]T. D. Rossing and N. H. Fletcher, *Principles of Vibration and Sound* (Springer, 2004).
[14]C. Lee, S. Kawano, T. Itoh, and T. Suga, J. Mater. Sci. **31**(17), 4559 (1996).
[15]C. Lee, T. Itoh, R. Maeda, and T. Suga, Rev. Sci. Instrum. **68**(5), 2091 (1997).
[16]T. Kobayashi, R. Maeda, T. Itoh, and R. Sawada, Appl. Phys. Lett. **90**(18), 183514 (2007).
[17]S. Shelton, M.-L. Chan, H. Park, D. Horsley, B. Boser, I. Izyumin, R. Przybyla, T. Frey, M. Judy, and K. Nunan, paper presented at the IEEE International Ultrasonics Symposium (IUS) (2009).
[18]J. Jung, S. Kim, W. Lee, and H. Choi, J. Micromech. Microeng. **23**(12), 125037 (2013).